Toward Predicting Changes in the Land Monsoon Rainfall a Decade in Advance

BIN WANG,[a,b,c] JUAN LI,[a,b,c] MARK A. CANE,[d] JIAN LIU,[e,f] PETER J. WEBSTER,[g] BAOQIANG XIANG,[h,i] HYE-MI KIM,[j] JIAN CAO,[a,b,c] AND KYUNG-JA HA[k,l]

[a] *Department of Atmospheric Sciences, University of Hawai'i at Mānoa, Honolulu, Hawaii*
[b] *International Pacific Research Center, School of Ocean and Earth Science and Technology, University of Hawai'i at Mānoa, Honolulu, Hawaii*
[c] *Earth System Modeling Center, Nanjing University of Information Science and Technology, Nanjing, China*
[d] *Lamont-Doherty Earth Observatory of Columbia University, Palisades, New York*
[e] *Key Laboratory of Virtual Geographic Environment, Ministry of Education, School of Geography Science, Nanjing Normal University, Nanjing, China*
[f] *Jiangsu Provincial State Key Laboratory Cultivation Base of Geographical Environment Evolution, School of Geography Science, Nanjing Normal University, Nanjing, China*
[g] *School of Earth and Atmospheric Sciences, Georgia Institute of Technology, Atlanta, Georgia*
[h] *NOAA/Geophysical Fluid Dynamics Laboratory, Princeton, New Jersey*
[i] *University Corporation for Atmospheric Research, Boulder, Colorado*
[j] *School of Marine and Atmospheric Sciences, Stony Brook University, Stony Brook, New York*
[k] *Department of Atmospheric Sciences, Pusan National University, Busan, South Korea*
[l] *Center for Climate Physics, Institute for Basic Science, Busan, South Korea*

(Manuscript received 4 August 2017, in final form 3 January 2018)

ABSTRACT

Predictions of changes of the land monsoon rainfall (LMR) in the coming decades are of vital importance for successful sustainable economic development. Current dynamic models, though, have shown little skill in the decadal prediction of the Northern Hemisphere (NH) LMR (NHLMR). The physical basis and predictability for such predictions remain largely unexplored. Decadal change of the NHLMR reflects changes in the total NH continental precipitation, tropical general circulation, and regional land monsoon rainfall over northern Africa, India, East Asia, and North America. Using observations from 1901 to 2014 and numerical experiments, it is shown that the decadal variability of the NHLMR is rooted primarily in (i) the north–south hemispheric thermal contrast in the Atlantic–Indian Ocean sector measured by the North Atlantic–south Indian Ocean dipole (NAID) sea surface temperature (SST) index and (ii) an east–west thermal contrast in the Pacific measured by an extended El Niño–Southern Oscillation (XEN) index. Results from a 500-yr preindustrial control experiment demonstrate that the leading mode of decadal NHLMR and the associated NAID and XEN SST anomalies may be largely an internal mode of Earth's climate system, although possibly modified by natural and anthropogenic external forcing. A 51-yr, independent forward-rolling decadal hindcast was made with a hybrid dynamic conceptual model and using the NAID index predicted by a multiclimate model ensemble. The results demonstrate that the decadal changes in the NHLMR can be predicted approximately a decade in advance with significant skills, opening a promising way forward for decadal predictions of regional land monsoon rainfall worldwide.

1. Introduction

Increasing demands of infrastructure planning, water resource management, disaster mitigation, and sustainable development require skillful predictions of the changes in land monsoon rainfall (LMR) a decade in advance. Forecasting such changes requires knowledge and understanding of anthropogenic forcing as well as large-amplitude natural decadal variability (Meehl et al. 2014). Some progress has been made in projecting the impacts of anthropogenic climate change on LMR (Meehl et al. 2007; Lee and Wang 2014). However, the mechanisms responsible for the natural decadal variability of LMR, which often overwhelms the anthropogenic trend on decadal time scales, remain elusive.

Denotes content that is immediately available upon publication as open access.

Corresponding author: Juan Li, juanl@hawaii.edu, and Jian Liu, jliu@njnu.edu.cn

DOI: 10.1175/JCLI-D-17-0521.1

Progress has been made in documenting and understanding decadal variations in monsoon precipitation in individual monsoon regions (Webster et al. 1998; Sutton and Hodson 2005; Goswami et al. 2006; Lu et al. 2006; Meehl and Hu 2006; Zhang and Delworth 2006). Furthermore, such predictions would allow for ''strategic adaptation,'' whereby extreme periods could be anticipated and their impacts mitigated (Webster and Jian 2011). However, the decadal variations and response to external forcing often occur beyond regional scales, such that a regional approach is unable to identify coherent, decadal changes and overriding, planetary-scale controls (Yim et al. 2014). Recent studies have examined the total global and Northern Hemisphere (NH) monsoon rainfall over both ocean and land during the short period of 1979–2012 (Wang et al. 2012, 2013). Because the oceanic monsoon rainfall far exceeds that over land, it remains unclear how the rainfall varies over land alone, the part most relevant for addressing societal concerns and needs. In addition, previous studies of the global-scale LMR could not differentiate between the trends associated with anthropogenic forcing and those related to natural climate variability due to the relatively short record used (Wang and Ding 2006; Zhou et al. 2008).

Direct decadal predictions of precipitation in some of the models from phase 5 of the Coupled Model Intercomparison Project (CMIP5) have shown some skill over the Sahel, midlatitude Eurasia, and parts of North America and southern South America (Bellucci et al. 2013; Gaetani and Mohino 2013; Martin and Thorncroft 2014; Meehl et al. 2014; Bellucci et al. 2015; Otero et al. 2016), but part of the positive skill found after 1980 can be attributed largely to specified atmospheric greenhouse gas concentration variations (Doblas-Reyes et al. 2013). Decadal predictions have shown some skill in forecasting 4-yr mean Sahel rainfall with lead times of 2–5 yr, but the skill is not statistically significant ($p \approx 0.2$) (van Oldenborgh et al. 2012). Prediction of LMR beyond the Sahel region has not been attempted before.

It is generally recognized that the variability on longer time scales often involves a larger spatial scale. However, the spatial scales of the coherent decadal variation of LMR, especially the dependence of decadal predictability on spatial scales, are unknown. The fundamental forms of decadal variability of LMR and the physical basis for decadal prediction of LMR have not been established, and the potential decadal predictability of LMR has yet to be estimated. The present study focuses primarily on the Northern Hemisphere LMR (NHLMR) because it has profound impacts on the global hydroclimate, and the NH monsoon region is home to about two-thirds of the world's population, particularly in less-developed countries that are often stressed by agricultural and urban water shortages; the latter is exacerbated by rapid urbanization, and both are affected by population growth.

In section 2, we describe the data and coupled climate model, numerical experiments, and the decadal prediction and validation methods used in this study. Section 3 discusses the rationale and physical meaning of the NHLMR index, a quantitative measure of the variability of NHLMR. Section 4 shows the origins of the decadal variability of the NHLMR are rooted in the North Atlantic–south Indian Ocean dipole (NAID) and extended El Niño–Southern Oscillation (XEN). In section 5, the physical basis for the decadal prediction of the NHLMR is discussed based on two sets of numerical experiments. Section 6 presents the skills of the decadal prediction of the NHLMR index using a hybrid dynamic conceptual model and the predictability estimation. The final section presents concluding remarks.

2. Data, model, experiments, and methodology

a. Data and decadal variation component

To examine the observed decadal–multidecadal variation, we used several long-record datasets:

(i) The monthly precipitation over global land from the Climatic Research Unit (CRU) time series version 3.23 (TS3.23) analysis, with a resolution of 0.5° × 0.5° during 1901–2014 (Harris et al. 2014).
(ii) The monthly precipitation derived from a historical, reconstructed precipitation dataset, with a resolution of 5° × 5° for 1901–2008 [twentieth century (20C) reconstructed precipitation] (Smith et al. 2010).
(iii) The monthly data of 850-hPa wind taken from the Twentieth Century Reanalysis (Compo et al. 2011), with a resolution of 2° × 2° for 1901–60.
(iv) The monthly circulation data derived from combined ERA-40 (Uppala et al. 2005) and ERA-Interim (Dee et al. 2011) data for 1958–2014.
(v) The monthly mean blended SST from the Hadley Centre Sea Ice and Sea Surface Temperature dataset (Rayner et al. 2003), with a resolution of 1° × 1° (1901–2014), and the NOAA Extended Reconstructed SST version 4 (Huang et al. 2016), with a resolution of 2° × 2° for 1901–2014.

To make these spatial resolutions comparable, we regridded all datasets using a uniform resolution of 2.5° × 2.5°.

To focus on the decadal–multidecadal variation, we used 4-yr running mean time series. The 4-yr running

mean is a widely used convention in the identification of decadal variability (Kim et al. 2012; van Oldenborgh et al. 2012; Goddard et al. 2013). For the 4-yr running mean time series, the yearly mark represents the second year of the 4-yr mean period; statistical tests for correlation coefficients are determined by the effective degrees of freedom by taking into account autocorrelations (Livezey and Chen 1983).

b. *Coupled climate model and numerical experiment designs*

Considering the strong air–sea interactions over the monsoon regions, we use a coupled climate model, the Nanjing University of Information Science and Technology (NUIST) coupled Earth System Model (NUIST-ESM) (Cao et al. 2015, 2017), to conduct numerical experiments. The low-resolution version of NUIST-ESM version 1a (v1a) was used, which consists of the Nucleus for European Modelling of the Ocean (NEMO, version 3.4) model (Madec 2008); ECHAM (version 5.3), which is directly coupled with a simple land surface model (Roeckner et al. 1996); the CICE (version 4.1) sea ice model (Hunke and Lipscomb 2010); and the Ocean Atmosphere Sea Ice Soil, version 3 (OASIS3)–Model Coupling Toolkit version 3.0 (MCT_3.0) coupler (OASIS3-MCT_3.0; Craig et al. 2017). The horizontal resolution of the atmospheric component is spectral T42, and there are 31 vertical levels. The ocean model also has 31 levels, and its horizontal resolution is $2° \times 2°$, with an increased resolution of $1/3°$ in the meridional direction in the equatorial region.

Two sets of numerical experiments were conducted. The first is a 500-yr uninitialized preindustrial experiment, which follows the CMIP5 (Taylor et al. 2012) protocol. The external forcings, including solar, volcanic, greenhouse gases, and land use/land cover, were fixed at the conditions at AD 1850. The purpose of this experiment is to identify the internal modes of the coupled climate system arising from the internal feedback processes among the atmosphere, ocean, land, and sea ice.

The second set of experiments consists of coupled integrations in which SST anomalies (SSTAs) associated with observed NAID and XEN indices act as a forcing to the atmosphere through nudging SST in the coupled climate model, while the external forcings (solar, volcanic, and greenhouse gases) are fixed at 1990 conditions. The purpose of this experiment is to simulate the steady response of the monsoon precipitation and circulation to a given NAID and XEN SSTA forcing. Following Alexander et al. (2002), only the SSTAs in the tropics (between 25°S and 25°N in the Pacific and between 30°S and 30°N in the North Atlantic–south Indian Ocean) are strongly nudged to the observed XEN or NAID patterns, while the atmosphere–ocean interaction is allowed to determine the SSTAs outside the forcing regions. Buffer zones with a width of 5° latitude–longitude along the nudged SSTA boundaries were used to obtain smoothed solutions.

Each forced experiment includes a 40-yr integration, and the result of each year is considered as one ensemble member, so the 40-member ensemble mean is used to suppress internal variability. For each set of the forced experiments, we conducted a pair of experiments in which two sets of ensemble simulations (each with 40 members) were made with opposite polarities in the NAID and XEN SSTA forcing. The differences between the two-ensemble means are taken as the atmospheric responses to the NAID and XEN SST anomalies. As a result, the SST anomaly over the forcing region is similar to observation, but the amplitude is nearly doubled.

In the SSTA forcing experiments, the SSTA in the specified regions was nudged toward the corresponding observed anomaly ∂SST superimposed on the model climatology SST_m by adding an additional SST tendency term in the uppermost level of the ocean temperature equation, $\partial\mathrm{SST}/\partial t_{\mathrm{nudging}} = [(\mathrm{SST}_{\mathrm{mc}} + \partial\mathrm{SST}) - \mathrm{SST}_m]/(1/2\ \mathrm{day})$, where $\mathrm{SST}_{\mathrm{mc}}$ is the model's climatological SST in the freely coupled run, ∂SST represents the observed regressed SST anomalies with reference to the two proposed SST indices, and SST_m is the model-simulated SST at each time step. The nudging time scale is short: one-half day. The resultant precipitation differences (between the paired opposite polarities sensitivity experiments) are considered to be the effects of the SSTA in the nudged (or forced) regions together with the atmosphere–ocean interaction that modify the local and remote forcing effects.

c. *Hybrid dynamic conceptual forecast model, IFR prediction method, and forecast skill measures*

A hybrid dynamic conceptual forecast model was built to predict decadal variations of the NHLMR. The dynamic conceptual model takes a two-tier approach in which a conceptual model is first derived from observations that link the NHLMR and SSTA indices, and then the SST indices predicted by the multidynamic model ensemble mean are used to predict the NHLMR.

An independent forward-rolling (IFR) prediction method was used for decadal prediction (e.g., Wang et al. 2015). Specifically, a "60 yr–10 yr" IFR prediction was made. Here, 60 yr is the training period, and 10 yr is the prediction period. Note that the conceptual prediction model is derived using only the 60 yr of data prior

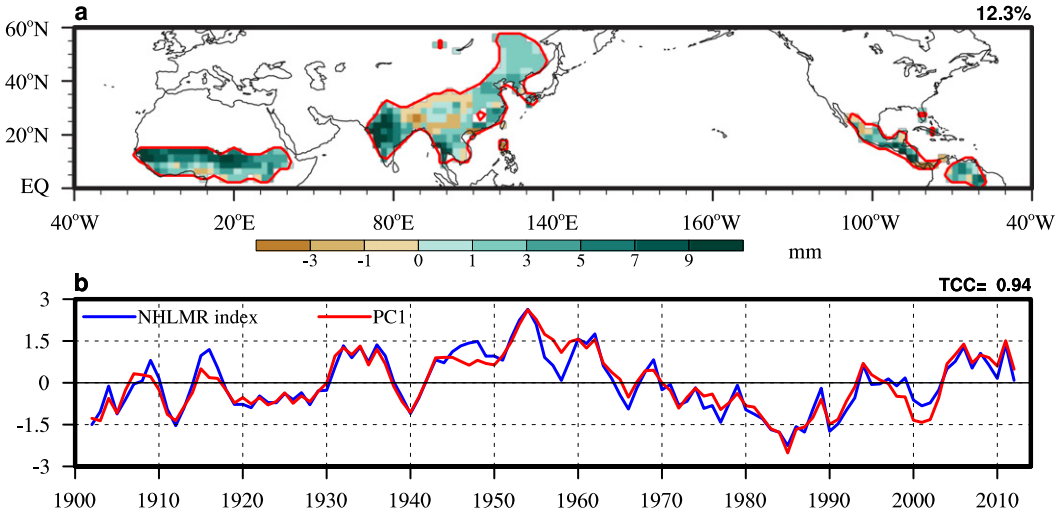

FIG. 1. Leading decadal mode of NH land summer monsoon rainfall variability (1901–2014). (a) Spatial pattern of the first EOF mode of the 4-yr running mean summer (MJJAS) rainfall and (b) the corresponding principal component (PC1; red line). The yearly mark on the x axis represents the second year of the 4-yr running mean. For comparison, the normalized decadal NHLMR (blue line) index is also plotted. The NHLMR index is the area-weighted average of the summer precipitation within the NH land monsoon domains (outlined by the red contours), which are defined by the regions where the local summer-minus-winter precipitation exceeds 300 mm, and the local summer precipitation exceeds 55% of the annual total. Here, summer is MJJAS, and winter is November–March. The insignificant least squares linear trends were removed before performing EOF analysis.

to the initial date of the dynamical prediction, and the forecast was made for the ensuing 10 yr. For instance, for the prediction initialized in 1961, we derived the conceptual prediction model using only the data from 1901 to 1960 and then predicted the NHLMR for the ensuing 10-yr period of 1961–70 so that a set of 4-yr-mean predictions could be obtained: that is, years 1–4 (1961–64), years 2–5 (1962–65), . . . , years 7–10 (1967–70). Similarly, we used data from 1902 to 1961 to predict the ensuing 10-yr (1962–71) forecast, and so on. Note that the conceptual model derived in the IFR prediction method does not use any information from the prediction period; thus, the conceptual model is free of artificially built-in skill. In this sense, the prediction is independent, so that the IFR prediction provides a more rigorous statistical test than the conventional cross-validation method.

To measure deterministic forecast skill, we used the correlation skill and the mean square skill score (MSSS) (Murphy 1988; Goddard et al. 2013). The MSSS reflects the percentage reduction in the mean square error (MSE) of the model forecast, compared to the MSE of the "climatological forecast," $\mathrm{MSE}_c = n^{-1}\sum_{i=1}^{n}(x_i - \bar{x})^2$. The MSSS is defined as

$$\mathrm{MSSS} = 1 - \frac{\mathrm{MSE}}{\mathrm{MSE}_c}.$$

Here, the mean square error of forecasts is defined as

$$\mathrm{MSE} = \frac{1}{n}\sum_{i=1}^{n}(f_i - x_i)^2,$$

where x_i and f_i denote the time series of the observations and forecasts, respectively. A positive (negative) skill indicates that the model forecast is better (worse) than the climatological forecast.

3. The NHLMR index

a. Definition of NHLMR index

Following Wang and Ding (2008) and Lee and Wang (2014), the NH land monsoon regions are defined by the regions where the local summer-minus-winter precipitation exceeds 300 mm, and the local summer precipitation exceeds 55% of the annual total (outlined by the red contours in Fig. 1a). Here, summer is May–September (MJJAS), and winter is November–March. The monsoon precipitation domain in NH includes four regional monsoons over northern Africa, South Asia, East Asia, and North America (Fig. 1a).

Figure 1a presents the spatial pattern of the leading empirical orthogonal function (EOF) mode of the decadal variation of the summer (May–September) monsoon precipitation over the NH land monsoon regions for the period of 1901–2014. The dominant mode of the 4-yr running mean NH summer LMR shows a nearly uniform spatial pattern across all of the NH land monsoon

regions, including northern Africa, South Asia, East Asia, Central and North America, and Venezuela, suggesting decadal variation of LMR may occur on a hemispheric scale.

The spatial coherency in the leading mode indicates that the intensity of the NH summer LMR can be measured meaningfully by the summer mean precipitation averaged over the entire NH land monsoon domain, as outlined by the red curves in Fig. 1a. We, therefore, introduce an NHLMR index defined as the area-weighted average of the summer mean precipitation over the entire NH land monsoon domain. The NHLMR index is computed from the CRU dataset. The same index computed from the 20C reconstructed precipitation is highly correlated ($r = 0.95$) with it, lending confidence to the values of the CRU rainfall index.

The NHLMR index represents the leading principal component of the NHLMR variability ($r = 0.94$; Fig. 1b). Because the summer monsoon rainfall dominates the corresponding annual mean rainfall, the yearly total rainfall from May to the next April (referred to as the "monsoon year"; Meehl 1987; Yasunari 1991) is highly correlated with the summer rainfall ($r = 0.96$); thus, the NHLMR represents not only the variation of summer rainfall, but also the variation of annual precipitation. In this study, the 4-yr running mean NHLMR is referred to as the decadal variation in the NHLMR or, simply, the decadal NHLMR.

The decadal NHLMR index displays large-amplitude fluctuations with a percentage change of up to 3.6% decade^{-1} (Fig. 1b), which is much larger than the corresponding trend induced by anthropogenic forcing (only approximately 0.5% decade^{-1}) projected by the CMIP5 multimodel ensemble under the representative concetration pathway 4.5 (RCP4.5) scenario (Lee and Wang 2014). The result here suggests that decadal variation might have a major contribution to the total precipitation change on a time scale of a few decades.

b. *Relationship between NHLMR and circulation, hydrology, and regional monsoons*

The NHLMR index measures interannual and decadal variations of the tropical general circulation. The year-to-year variation of the NHLMR index correlates well with interannual variations of the summer mean intensities of the tropical monsoon circulation ($r = 0.87$, $p < 0.01$) and the Walker circulation ($r = -0.69$, $p < 0.01$; Figs. 2b and 2c, respectively). Here, the tropical monsoon circulation intensity is measured by the vertical shear of the zonal wind (850- minus 200-hPa zonal wind) averaged over 0°–20°N, 120°W–90°E (Wang et al. 2013), and the intensity of the Walker circulation is measured by the low-level zonal winds at 850 hPa averaged over the equatorial Pacific (10°S–10°N, 140°E–140°W).

The NHLMR index is a good indicator for the NH hydrological cycle. The decadal NHLMR index is highly correlated with the decadal variation of the total precipitation over the entire NH land region between the equator and 60°N ($r = 0.83$, $p < 0.01$; Fig. 2a). Note, however, that the total amount of the precipitation averaged over the NH land regions has an increasing trend that comes primarily from the nonmonsoonal, mid-to-high-latitude regions.

The decadal NHLMR index also reflects well the decadal variations of its four regional components over northern Africa, South Asia, East Asia, and North America. The results in Fig. 3 show that the leading EOF modes of the four NH regional monsoons (northern Africa, India, East Asia, and North America), similar to the NHLMR, also exhibit nearly uniform variability, but they account for a much higher fractional variance than the NHLMR, especially over northern Africa and India, where the leading modes account for 38% and 34% of the total variance, respectively. The summer mean rainfall averaged over each regional monsoon domain can be used to define the corresponding regional LMR indices. These regional LMR indices represent the corresponding regional leading modes well with correlation coefficients varying from 0.76 to 0.97. Note that the decadal NHLMR is significantly correlated with the decadal variations of all four regional LMR indices with significant ($p < 0.01$) correlation coefficients ranging from 0.51 to 0.73 (Table 1). Therefore, understanding the sources of predictability of the NHLMR may provide useful information for understanding of decadal predictions of the individual regional LMR, and vice versa.

4. Sources of the decadal variability of the NHLMR

To detect potential causes of decadal variability, we explore how the NHLMR is linked to decadal variations in the global SST. Figure 4 shows the correlation map of the 4-yr running mean SSTA and the decadal NHLMR during the period of 1901–2014. The SSTA pattern features a grand east–west contrast in the Pacific and a north–south hemispheric contrast in the Atlantic and Indian Ocean sector. Over the Atlantic and Indian Oceans, the SSTA associated with an intensified NHLMR features a warm North Atlantic (NA) and cold south

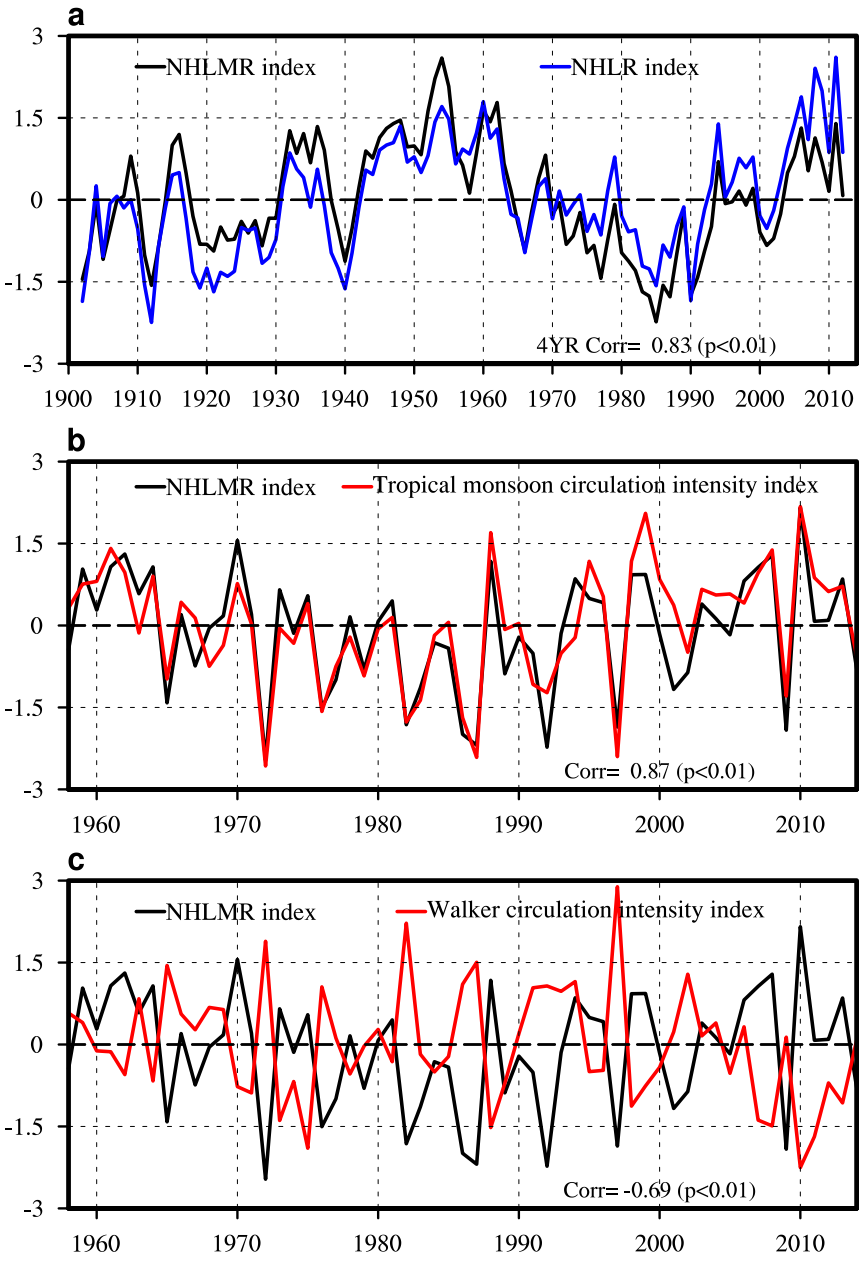

FIG. 2. NHLMR index and tropical general circulation intensity. (a) The decadal NHLMR index (black) and the 4-yr running mean NH land rainfall (NHLR) index (blue), which is the MJJAS mean precipitation averaged over the NH land areas between 0°and 60°N. (b) The year-to-year variations of the tropical monsoon circulation intensity index (red) measured by the vertical shear of zonal wind (850- minus 200-hPa zonal wind) averaged over 0°–20°N, 120°W–90°E. (c) The year-to-year variations of the Walker circulation intensity index (red) measured by the low-level zonal winds at 850 hPa averaged over the equatorial Pacific (10°S–10°N, 140°E–140°W). All time series are normalized by their corresponding standard deviations. The correlation coefficients and the corresponding statistical significance levels are shown at the bottom of each panel. Combined ERA-40 and ERA-Interim dataset for 1958–2014 is used to calculate the circulation intensities.

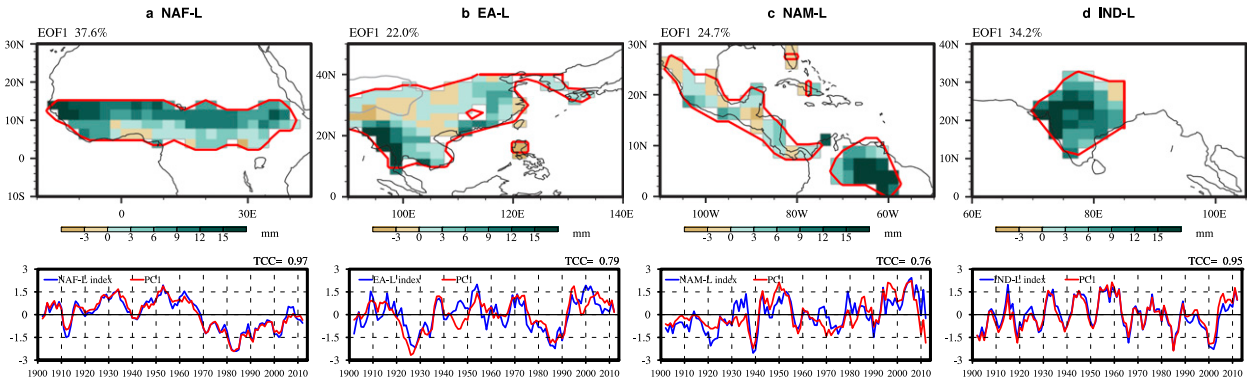

FIG. 3. (a) The leading EOF modes of regional summer LMR decadal variability during 1901–2014 after 4-yr running average. (top) The spatial pattern and (bottom) the corresponding principal component (PC1; red line) of the first EOF mode of the summer (MJJAS) mean rainfall over the NAF-L region. For comparison, the northern African summer LMR index (blue line) is also plotted in the bottom panel with the temporal correlation coefficient (TCC) shown in the top-right corner. (b)–(d) As in (a), but for EA-L, NAM-L, and IND-L, respectively.

Indian Ocean (SIO). To quantify this characteristic pattern, we define a NAID index:

$$\text{NAID index} = \text{SSTA(NA)} - \text{SSTA(SIO)},$$

which is the SSTA averaged over the NA (0°–60°N, 80°W–0°) minus that averaged over the SIO (0°–40°S, 50°–110°E), as illustrated in Fig. 4. The decadal variation of the NAID index is significantly correlated with the decadal NHLMR index ($r = 0.68$, $p < 0.01$; Fig. 5a).

Note here that both the averaged SST anomaly for the North Atlantic (0°–60°N, 0°–80°W) (Enfield et al. 2001) and the SST anomalies averaged over the SIO have significant upward trends, and individually they are not significantly related to the NHLMR index (Fig. 6). In contrast, their difference, the NAID index, has no appreciable trend and correlates significantly with the decadal NHLMR.

The NAID index represents not only the contrasting SSTA between the NA and SIO, but also the north–south hemispheric SSTA contrast in the Atlantic–Indian Ocean sector, denoted by the NASIOSA index and calculated by 2 × NA SSTA − SIO SSTA − SA SSTA, where SA is the South Atlantic (0°–40°S). This alternative index is highly correlated with the NAID index ($r = 0.94$, $p < 0.01$). Both the NAID and NASIOSA indices are significantly correlated with the NHLMR index (Fig. 5a). Basically, use of either index yields the same prediction results.

How can the NAID affect the NHLMR? The NAID dominates the overall north–south hemispheric SST contrast because the Pacific SSTA is primarily an east–west contrast (Fig. 4), and the north–south hemispheric contrast in the Pacific is not significantly correlated with the NHLMR index ($r = 0.32$, $p > 0.05$). It has been shown that the NHLMR can be changed by the interhemispheric SST gradients–induced, low-level, northward cross-equatorial flows (Liu et al. 2009, 2012; Wang et al. 2013). A positive phase of NAID combines the effects of a warm NA and cold SIO. The warm NA can shift the intertropical convergence zone northward (Schneider et al. 2014) and enhance the North American monsoon (Sutton and Hodson 2005; Meehl and Hu 2006), the West African monsoon (Gaetani and Mohino 2013; Martin and Thorncroft 2014; Otero et al. 2016), and Asian rainfalls (Lu et al. 2006; Meehl and Hu 2006; Zhang and Delworth 2006). A cold south Indian Ocean can enhance the northward temperature gradient between the Indian Ocean and the Asian continent, strengthening the Asian monsoon rainfall (Webster et al. 1998).

The principal Pacific decadal SST anomaly is characterized by an east–west contrast resembling the interdecadal Pacific oscillation (IPO) (Power et al. 1999) and mega-ENSO (Wang et al. 2013). Following Wang et al. (2013), we use a new index to measure mega-ENSO that is given by the SSTA averaged over the western Pacific

TABLE 1. The correlation coefficients between the NHLMR index and northern African LMR (NAF-L) index, East Asian LMR (EA-L) index, North American LMR (NAM-L) index, and Indian LMR (IND-L) index during 1901–2014. All correlation coefficients are significant at 0.01 significant level, taking autocorrelations into account. These regional summer (MJJAS) monsoon rainfall indices are defined by the areal means in the corresponding monsoon domains (Fig. 3).

TCC	NAF-L index	EA-L index	NAM-L index	IND-L index
NHLMR index	0.73	0.56	0.51	0.67

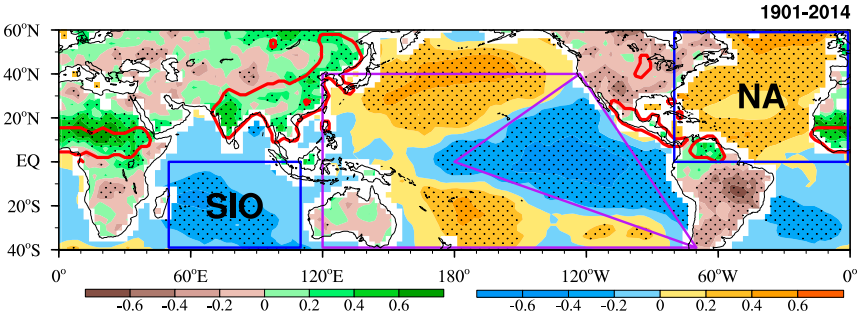

FIG. 4. SSTAs associated with the decadal NHLMR index. The correlation map of boreal summer (MJJAS) SST (shading over the ocean) and land rainfall (shading over the land) with respect to the decadal NHLMR index during 1901–2014. The monsoon land areas are outlined in red. The blue and purple lines outline the areas used for defining the NAID and XEN indices, respectively. The correlation coefficients that are significant at a 95% confidence level by a Monte Carlo test (Hope 1968) are dotted.

(WP) K-shaped region minus that over the eastern Pacific (EP) triangle region, as shown in Fig. 4. This new index is referred to as the XEN index:

$$\text{XEN index} = \text{SSTA(WP K-shaped region)} - \text{SSTA(EP triangle region)}.$$

The XEN is a multi–time scale index: On the interannual time scale, it is highly correlated with the Niño-3.4 index ($r = 0.91$ for 1958–2010; Wang et al. 2013); on the decadal time scale, it is well correlated with the Pacific decadal oscillation (PDO) (Mantua et al. 1997), with $r = -0.82$ (Wang et al. 2013).

The decadal variation of the XEN index is significantly correlated with the decadal NHLMR index ($r = 0.53$, $p < 0.05$; Fig. 5b). Physically, the eastern Pacific cooling and western Pacific warming are consistent with a strengthening of the two Pacific subtropical highs in the Northern and Southern Hemispheres and their associated trade winds, causing moisture to converge into the Asian and African monsoon regions and, thus, contributing to the intensification of NHLMR.

The combination of the NAID and XEN indices can simulate the decadal NHLMR index when used as "predictors" in a regression model. Using the observed data from 1901 to 2014, we find

$$\text{NHLMR index} = 0.59 \times \text{NAID} + 0.37 \times \text{XEN},$$

where the NAID and XEN explain, respectively, 35% and 14% of the NHLMR variance.

The relationship between the NHLMR and the two global SST indices has remained steady over the past 114 years. Figure 7a shows the correlation map of the 4-yr running mean SST anomalies and the decadal NHLMR during the period of 1901–60. The SSTA pattern associated with the NHLMR during 1901–60 bears close similarity to that for the period of 1901–2014 (Fig. 4). If we use the data from 1901 to 1960 to derive the conceptual model, we can reconstruct the decadal NHLMR for the ensuing 64-yr period (1961–2014) with observed SST during the latter period. The temporal correlation skill is $r = 0.71$ ($p < 0.05$) and MSSS = 0.40 (Fig. 7b). This suggests that the relationship found for the period of 1901–60 is statistically stationary across the entire data record from 1901 to 2014. This steady linkage between the NHLMR and NAID is essential for the independent forecast made later in section 6.

5. Physical basis for the decadal predictability of the NHLMR: Numerical experiments

The link between the NHLMR and NAID/XEN suggests that the decadal variability of the NHLMR may be rooted in the hemispheric thermal contrast in the Atlantic and Indian Ocean sector and the east–west thermal contrast in the Pacific. Here, we show that the decadal variations in SST associated with the NAID and XEN can reproduce observed decadal variations in the NHLMR, and the decadal variations of the NHLMR, NAID, and XEN are likely intrinsic modes of the climate variability in the coupled climate system.

a. Results from perturbed coupled experiments

To confirm the proposed causality in the previous section and to understand the underlying physical processes by which the NAID and XEN SSTA impacts the NHLMR, we conducted a suite of coupled climate model experiments with the NUIST-ESM v1a model. The experimental designs were described in section 2.

The coupled model's ensemble simulations generally replicate the observed anomalous NH summer LMR

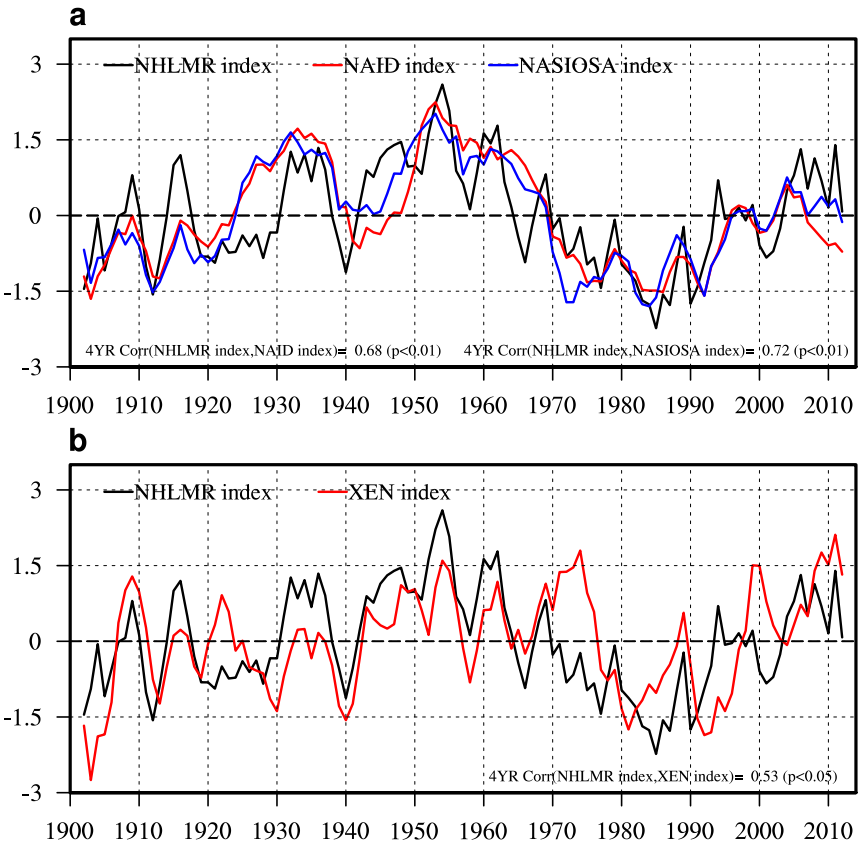

FIG. 5. Decadal SST indices from 1901–2014. Decadal variation (4-yr running mean) of (a) the NAID index (red), representing the thermal contrast between the North Atlantic and south Indian Ocean, the NASIOSA index (2 × NA SSTA − SIO SSTA − SA SSTA; blue), representing the north–south thermal contrast in the Atlantic and Indian Ocean sector, and (b) XEN index (red). For comparison, the NHLMR index is also plotted (black). All indices are normalized by their corresponding standard deviations.

(Fig. 8). With the nudged tropical NAID SSTA (Fig. 8b), the positive phase of the NAID forcing reproduces a weak central equatorial Pacific cooling (similar to observation; Fig. 8a), which, on one hand, generates westerly anomalies in the eastern Pacific that strengthen the North American summer monsoon, but on the other hand, enhances equatorial easterly over the western Pacific and the associated western North Pacific subtropical

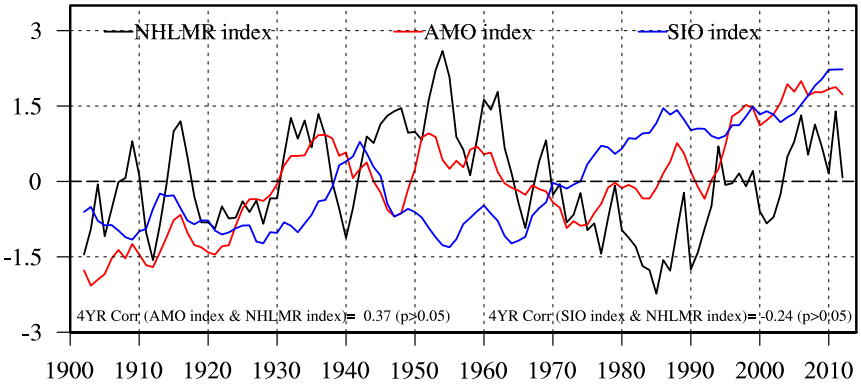

FIG. 6. Decadal variation (4-yr running mean) of undetrended Atlantic multidecadal oscillation (AMO) index, SIO SSTA index, and the NHLMR index.

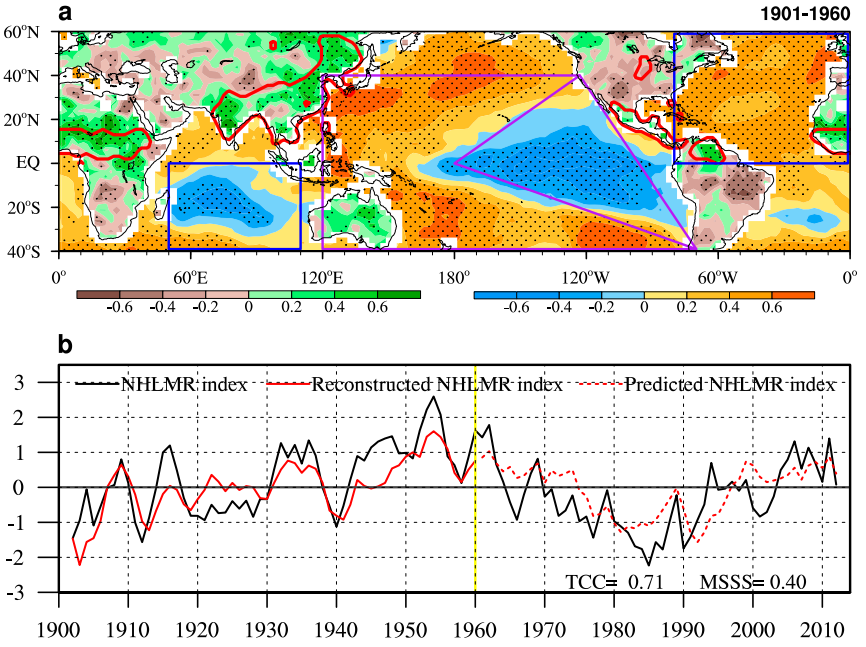

FIG. 7. (a) As in Fig. 4, but for the period of 1901–60. (b) The observed decadal NHLMR index (black line), the reconstructed decadal NHLMR index using the NAID and XEN indices during the training period of 1901–60 (solid red line), and the predicted decadal NHLMR index for the period of 1961–2014 (dashed red line). The TCC and MSSS score for the independent prediction period are shown in (b).

high (weaker than the observed), thereby strengthening the subtropical East Asian summer monsoon. The positive NAID forcing also leads to an enhanced northern African LMR, but the increased northern African rainfall is not accompanied by significant circulation anomalies, as it is in the observed counterpart.

With the nudged tropical XEN SSTA forcing (Fig. 8d), a mega La Niña reinforces Pacific trades and

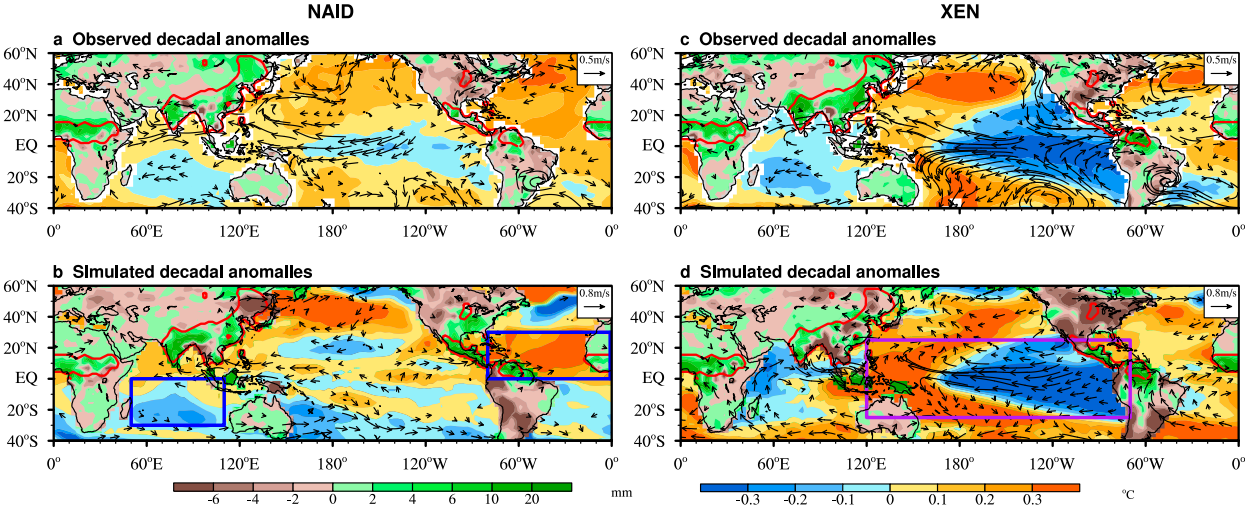

FIG. 8. Observed and coupled climate model-simulated decadal anomalies. (a) Observed summer (MJJAS) mean SSTAs over the ocean (shading; °C), precipitation anomalies over the land (shading; mm), and 850-hPa wind anomalies (vectors; m s^{-1}) that are regressed onto the NAID index for the period of 1901–60. (b) Model-simulated responses of SST, precipitation, and 850-hPa wind anomalies to the NAID SST forcing. (c),(d) As in (a),(b), but for the anomalies associated with the XEN index. The blue and purple boxes in (b) and (d), respectively, indicate the regions where the SSTs are nudged to observation.

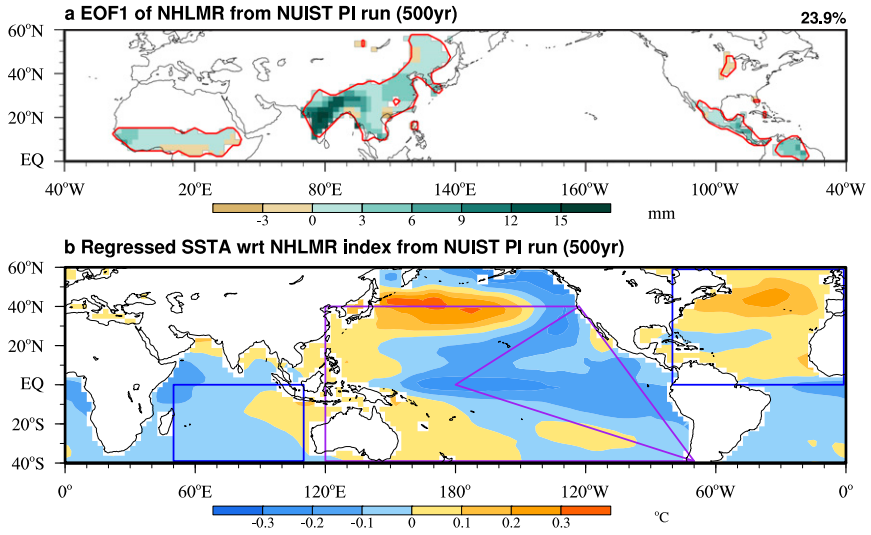

FIG. 9. Leading decadal mode of NHLMR variability and related SSTA from NUIST-ESM PI run (500 yr). (a) Spatial pattern of the first EOF mode of the 4-yr running mean NHLMR. (b) Regressed 4-yr running mean summer (MJJAS) SSTA with respect to the simulated decadal NHLMR index.

the associated Walker circulation, thereby increasing the moisture convergence and monsoon rainfall over Indonesia that further enhances the Indian southwest monsoon. But the simulated easterly anomalies are not as strong as the observed, and, consequently, the precipitation increase over East Asia is weaker than the observed. The mega La Niña also boosts the anomalous westerlies in the equatorial Atlantic through a tropical teleconnection, strengthening the West African monsoon. However, the increased rainfall in the North American land monsoon region (mainly over Venezuela) is due to the enhanced southerlies associated with the South Atlantic subtropical high, while in observation (Fig. 8c) the increased rainfall is linked to the anomalous easterlies and associated positive shear vorticity over the far eastern North Pacific. This discrepancy appears to be related to the significant SST errors simulated in the northeastern Pacific and subtropical southwest Atlantic (Fig. 8d).

The results here suggest that the decadal variability of the NHLMR is likely a result of the global SST anomalies associated with the NAID and XEN.

b. Results from unforced preindustrial control experiments

To examine whether the observed relationships between the NHLMR and the NAID/XEN can also be found in the long-term integrations with a coupled climate model, we performed a 500-yr preindustrial (PI) control experiment with the same NUIST model. The external forcing, including solar, volcanic, greenhouse gases, and land use/land cover, were fixed at conditions around AD 1850 following the CMIP5 (Taylor et al. 2012) PI protocol.

Similar to the observed NHLMR variations, the dominant mode of the 4-yr running mean NH summer LMR shows a nearly uniform spatial pattern across all NH land monsoon regions, with a heavy weight over India (Fig. 9a). The 4-yr running mean SST anomalies regressed onto the model decadal NHLMR index also show a similar pattern (Fig. 9b) as the observed (Fig. 4), except that the negative correlation area in the equatorial Pacific extended farther west, a consequence of the model's excessive cold tongue bias. The model-simulated NAID and XEN indices are significantly correlated with the NHLMR index, with the correlation coefficients of 0.53 ($p < 0.01$) and 0.55 ($p < 0.01$), respectively. In the unforced PI control run, the decadal variation of the NHLMR is a mode of internal variability. The result here suggests that the observed decadal variability of the NHLMR may be a result of the internal feedback processes within the coupled climate system, possibly modified by the external forcing in the twentieth century.

6. Decadal prediction of the NHLMR index using a hybrid dynamic conceptual model

We first show that the current global climate models may have little skill in the direct prediction of decadal variations of the NHLMR. This assertion is based on examination of three coupled climate models that participated

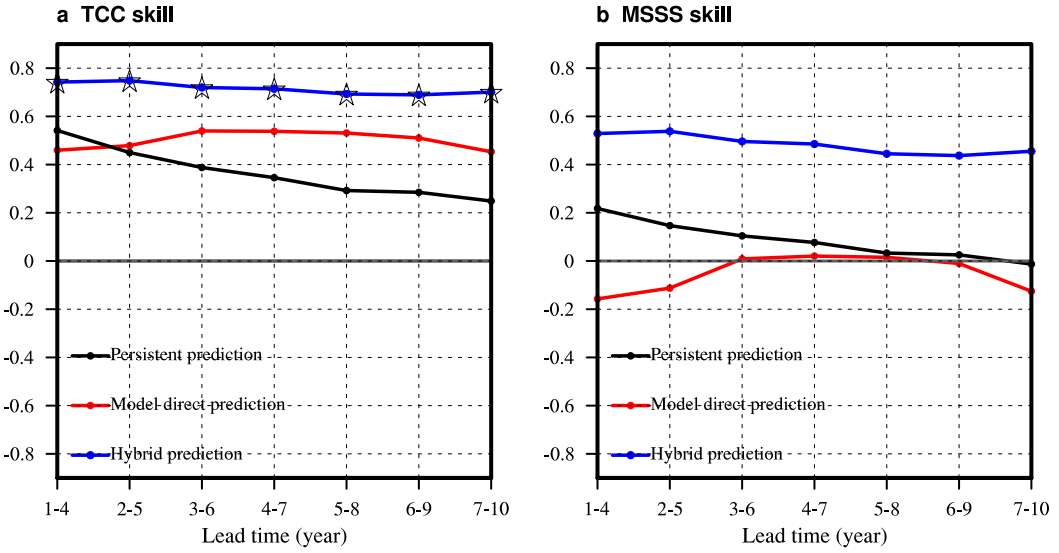

FIG. 10. Decadal hindcast skills for the NHLMR index. (a) TCC skill derived by hybrid dynamic conceptual forecast (blue), model direct rainfall prediction (red), and persistent prediction (black) as functions of the lead time (yr) for the period of 1967–2011 (i.e., the 4-yr running mean from 1968 to 2009). The hybrid forecast used the model-predicted NAID index only. Stars indicate that the TCC is significant at a 95% confidence level, taking serial autocorrelation into account. (b) As in (a), but for the MSSS.

in the CMIP5 decadal prediction experiment, including the Met Office Decadal Prediction System [based on the Hadley Centre Coupled Model, version 3 (HadCM3)]; the Geophysical Fluid Dynamics Laboratory (GFDL) Climate Model, version 2.1 (GFDL CM2.1); and the Max Planck Institute for Meteorology Earth System Model, low resolution (MPI-ESM-LR). Both HadCM3 and GFDL CM2.1 have 10-member ensembles, while MPI-ESM-LR has 3-member ensembles. The hindcasts consist of 51 sets of 10-yr retrospective predictions initialized every year from 1961 to 2011. As shown in Fig. 10b, the three-models' ensemble mean prediction of the NHLMR has a near-zero MSSS, suggesting that the skill is essentially the same as climatological forecast.

Because the NAID and XEN involve coupled atmosphere–ocean processes and slow ocean adjustment processes, they may be more predictable than the NHLMR on a decadal scale. Thus, we further assessed the three CMIP5 models' ensemble prediction of the decadal variation of the NAID and XEN. The results indicate that the NAID index can be predicted 7–10 yr in advance with useful skill, but the XEN index cannot (Fig. 11). Because the ensemble prediction smoothed out interannual variations, the predicted NAID tends to be dominated by decadal variations.

Unlike in the ideal experiments, where the nudged SST has a realistic pattern and the use of large-ensemble simulations avoids errors in the initial conditions, the SST patterns predicted by CMIP5 models are often less realistic, and the initial conditions have considerable errors. In addition, the models have difficulties in modeling accurate precipitation climatology and teleconnections linking SST forcing and monsoon circulation, as well as the atmosphere–ocean interactions in the monsoon regions that are critical for capturing monsoon variability (Wang et al. 2004, 2005). Thus, the direct decadal prediction of the NHLMR in the models has no skill, even though the models have useful skills in prediction of the NAID index. For this reason, a hybrid dynamic conceptual model approach is adopted here.

The dynamic conceptual model uses the conceptual model derived from observations that relates the NHLMR to the NAID as the sole predictor, and then uses the NAID index predicted by the ensemble mean of the three aforementioned dynamical models as the input predictor. We made a 60 yr–10 yr IFR prediction (section 2c). Figure 10 shows that a 51-yr hindcast of the 7–10-yr mean NHLMR index achieved a correlation skill of 0.70 ($p < 0.05$) and MSSS = 0.46, which is significantly higher than the corresponding dynamical models' direct rainfall prediction and a persistence forecast.

The IFR prediction provides an estimate of practical predictability, a constructive lower bound for the predictability of the NHLMR index. It suggests that about 50% of the decadal variance of the NHLMR can be achievable by using the proposed hybrid conceptual model. In the hybrid model prediction, the XEN index was not used because the models could not predict its decadal variation (Fig. 11b). If the model can capture

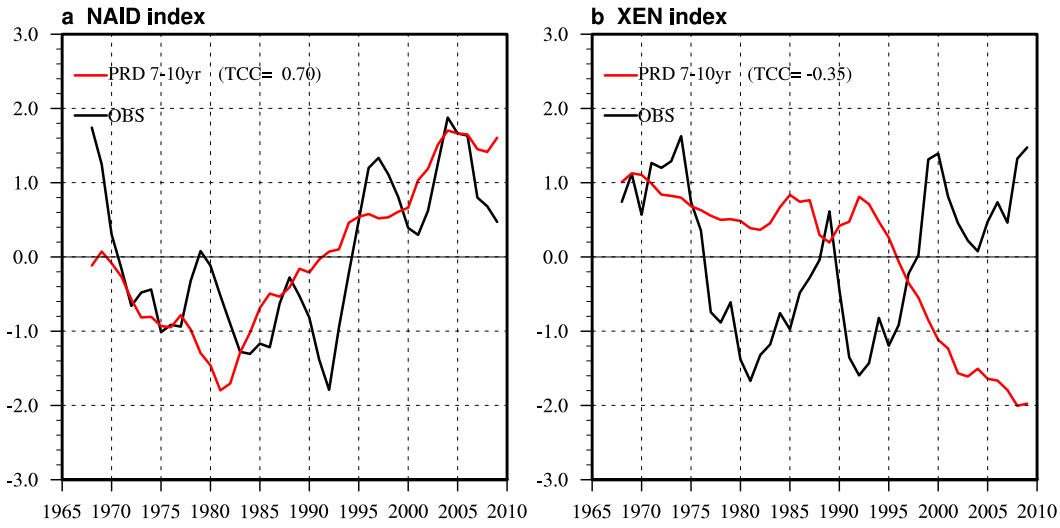

FIG. 11. (a) Normalized NAID index derived from observations (black line) and three-model multimodel ensemble (MME) hindcast with a 7–10-yr lead time (red line). (b) As in (a), but for the XEN index. The TCC during the 4-yr running mean period of 1968–2009 is indicated in parentheses.

decadal variation of the XEN, the achievable skill might be improved.

7. Concluding remarks

This pilot study explores decadal predictability of the LMR, which has profound societal impacts on some two-thirds of the global population. We find that the decadal variations in the LMR have a coherent structure across the entire NH monsoon domain, including the northern African, Indian, East Asian, and North American regional monsoons, so the spatial scale of decadal variability is beyond regional and at least on hemispheric continental scale (Fig. 1). The intensity change of the LMR averaged over the NH monsoon regions, measured by the NHLMR index, represents very well the decadal changes in the total amount of the NH land precipitation and the decadal changes in tropical monsoon circulation and Walker circulation (Fig. 2). The NHLMR index also represents the decadal rainfall variability in the four regional monsoons, with significant ($p < 0.01$) correlation coefficients ranging from 0.51 to 0.73, especially the northern African monsoon and Indian monsoon (Fig. 3 and Table 1). However, the current global climate models have shown little skill in the direct prediction of decadal variability of the NHLMR (Fig. 10b).

Using the observed data from 1901 to 2014 and numerical experiments with a coupled climate model (the NUIST-ESM v1a), we showed that the decadal predictability of the NHLMR is rooted primarily in decadal variations of the north–south hemispheric SSTA contrast in the Atlantic–Indian Ocean sector and augmented by an east–west SSTA contrast in the Pacific (Fig. 4). The former is characterized by a dipolar SST anomaly pattern between the NA and SIO (NAID) and the latter features a mega-ENSO pattern and is measured by the extended ENSO (XEN) index. Both indices are significantly correlated with the NHLMR index (Fig. 5). A set of SSTA nudged experiments indicates that the tropical SSTA associated with the NAID and XEN indices can reproduce, to a large extent, the observed NHLMR anomalies (Fig. 8), suggesting the decadal variability of the NHLMR is rooted in the two global SST modes: the NAID and XEN. A 500-yr unforced simulation with the NUIST-ESM v1a model demonstrates that the LMR over the NH has a coherent decadal variation pattern that is significantly correlated with NAID and XEN (Fig. 9), suggesting that the observed decadal variability of the NHLMR may be a result of the internal feedback processes within the coupled climate system, possibly modified by the natural and anthropogenic external forcing since 1900.

Using a conceptual model linking the NHLMR and NAID and three dynamical models' predicted NAID, we made a 51-yr decadal hindcast with an independent forward-rolling prediction method (section 2c). The hindcast results show that the 4-yr mean NHLMR can be predicted approximately a decade in advance, with significant correlation skill of 0.70 ($p < 0.05$) and MSSS = 0.46; both are significantly better than the direct dynamical prediction of the NHLMR and the persistent prediction (Fig. 10).

The decadal prediction made here provides an estimate of a constructive lower bound for the decadal

predictability of the NHLMR index. It suggests that about 50% of the decadal variance of the NHLMR can be predicted. Our results open a promising way forward for decadal predictions of regional land monsoon rainfall worldwide.

We have shown that the NHLMR depends on the north–south hemispherical SSTA contrast in the Atlantic–Indian Ocean sector. The mechanism responsible for this hemispheric asymmetric SST variation, however, remains elusive. The North Atlantic SST is likely driven by atmospheric noise and affected by radiative forcing (greenhouse gases and aerosols) (Bellomo et al. 2017; Bellucci et al. 2017; Cane et al. 2017; Murphy et al. 2017). The north–south thermal contrast in the Atlantic is suggested to be related to fluctuations in the Atlantic meridional overturning circulation (Liu 2012; McCarthy et al. 2015), although this mechanism remains subject to considerable debate (Liu 2012; Knudsen et al. 2014). The physical link between the South Atlantic and SIO SST variability is an open question. In addition to internal feedback processes, volcanic eruptions have been shown to have a significant influence on the decadal variability of NH monsoon rainfall (Liu et al. 2016). The variations in anthropogenic aerosol emissions have also been shown to have an impact on the large-scale meridional temperature gradients and the projection of the global-scale and regional monsoons (Polson et al. 2014; Guo et al. 2015). These issues call for further investigation.

This pilot study demonstrates that the decadal variations in the LMR can be predicted for the NH. Although the decadal variation of the NHLMR intensity is significantly correlated with the decadal LMR variabilities of the four regional (northern Africa, India, East Asia, and North America) monsoons, these regional LMR intensities are not solely driven by the NAID and XEN. Highly localized aerosol emission sources and the resultant loadings could have negative impacts on the regional monsoons. Exploration and implementation of SST predictors that reflect distinct sources of predictability of individual regional monsoons are imperative. A detailed regional approach to LMR prediction is underway.

Acknowledgments. This study is jointly supported by the National Natural Science Foundation of China (Grant 41420104002; J. Liu and B. W.), the National Key Research and Development Program of China (Grant 2016YFA0600401; J. Liu and B. W.), the Global Research Laboratory (GRL) Program of the National Research Foundation of Korea (Grant 2011-0021927; B. W. and K. H.), National Science Foundation Award 1638256 (P. W.), KMA R&D Program under Grant KMIPA 2016-6010 (H. K.), and NOAA's Climate Program Office, Climate Variability, and Predictability Program (GC14-252; B. X.) and IBS-R028-D1 (K. H.). This is publication 10293 of the School of Ocean and Earth Science and Technology, publication 1303 of the International Pacific Research Center, and publication 201 of the Earth System Modeling Center.

REFERENCES

Alexander, M. A., I. Bladé, M. Newman, J. R. Lanzante, N.- C. Lau, and J. D. Scott, 2002: The atmospheric bridge: The influence of ENSO teleconnections on air–sea interaction over the global oceans. *J. Climate*, **15**, 2205–2231, https://doi.org/10.1175/1520-0442(2002)015<2205:TABTIO>2.0.CO;2.

Bellomo, K., L. N. Murphy, M. A. Cane, A. C. Clement, and L. M. Polvani, 2017: Historical forcings as main drivers of the Atlantic multidecadal variability in the CESM large ensemble. *Climate Dyn.*, https://doi.org/10.1007/s00382-017-3834-3, in press.

Bellucci, A., and Coauthors, 2013: Decadal climate predictions with a coupled OAGCM initialized with oceanic reanalyses. *Climate Dyn.*, **40**, 1483–1497, https://doi.org/10.1007/s00382-012-1468-z.

——, and Coauthors, 2015: An assessment of a multi-model ensemble of decadal climate predictions. *Climate Dyn.*, **44**, 2787–2806, https://doi.org/10.1007/s00382-014-2164-y.

——, A. Mariotti, and S. Gualdi, 2017: The role of forcings in the twentieth-century North Atlantic multidecadal variability: The 1940–75 North Atlantic cooling case study. *J. Climate*, **30**, 7317–7337, https://doi.org/10.1175/JCLI-D-16-0301.1.

Cane, M., A. Clement, L. Murphy, and K. Bellomo, 2017: Low-pass filtering, heat flux, and Atlantic multidecadal variability. *J. Climate*, **30**, 7529–7553, https://doi.org/10.1175/JCLI-D-16-0810.1.

Cao, J., B. Wang, B. Xiang, J. Li, T. Wu, X. Fu, L. Wu, and J. Min, 2015: Major modes of short-term climate variability in the newly developed NUIST Earth System Model (NESM). *Adv. Atmos. Sci.*, **32**, 585–600, https://doi.org/10.1007/s00376-014-4200-6.

——, and Coauthors, 2017: The NUIST Earth System Model (NESM) version 3: Description and preliminary evaluation *Geosci. Model Dev. Discuss.*, https://doi.org/10.5194/gmd-2017-206.

Compo, G. P., and Coauthors, 2011: The Twentieth Century Reanalysis project. *Quart. J. Roy. Meteor. Soc.*, **137**, 1–28, https://doi.org/10.1002/qj.776.

Craig, A., S. Valcke, and L. Coquart, 2017: Development and performance of a new version of the OASIS coupler, OASIS3-MCT_3.0. *Geosci. Model Dev.*, **10**, 3297–3308, https://doi.org/10.5194/gmd-10-3297-2017.

Dee, D. P., and Coauthors, 2011: The ERA-Interim reanalysis: Configuration and performance of the data assimilation system. *Quart. J. Roy. Meteor. Soc.*, **137**, 553–597, https://doi.org/10.1002/qj.828.

Doblas-Reyes, F. J., and Coauthors, 2013: Initialized near-term regional climate change prediction. *Nat. Commun.*, **4**, 1715, https://doi.org/10.1038/ncomms2704.

Enfield, D. B., A. M. Mestas-Nuñez, and P. J. Trimble, 2001: The Atlantic multidecadal oscillation and its relation to rainfall and river flows in the continental U.S. *Geophys. Res. Lett.*, **28**, 2077–2080, https://doi.org/10.1029/2000GL012745.

Gaetani, M., and E. Mohino, 2013: Decadal prediction of the Sahelian precipitation in CMIP5 simulations. *J. Climate*, **26**, 7708–7719, https://doi.org/10.1175/JCLI-D-12-00635.1.

Goddard, L., and Coauthors, 2013: A verification framework for interannual-to-decadal predictions experiments. *Climate Dyn.*, **40**, 245–272, https://doi.org/10.1007/s00382-012-1481-2.

Goswami, B. N., M. S. Madhusoodanan, C. P. Neema, and D. Sengupta, 2006: A physical mechanism for North Atlantic SST influence on the Indian summer monsoon. *Geophys. Res. Lett.*, **33**, L02706, https://doi.org/10.1029/2005GL024803.

Guo, L., A. G. Turner, and E. J. Highwood, 2015: Impacts of 20th century aerosol emissions on the South Asian monsoon in the CMIP5 models. *Atmos. Chem. Phys.*, **15**, 6367–6378, https://doi.org/10.5194/acp-15-6367-2015.

Harris, I., P. D. Jones, T. J. Osborn, and D. H. Lister, 2014: Updated high-resolution grids of monthly climatic observations—The CRU TS3.10 dataset. *Int. J. Climatol.*, **34**, 623–642, https://doi.org/10.1002/joc.3711.

Hope, A. C. A., 1968: A simplified Monte Carlo significance test procedure. *J. Roy. Stat. Soc.*, **30B**, 582–598.

Huang, B., and Coauthors, 2016: Further exploring and quantifying uncertainties for Extended Reconstructed sea surface temperature (ERSST) version 4 (v4). *J. Climate*, **29**, 3119–3142, https://doi.org/10.1175/JCLI-D-15-0430.1.

Hunke, E. C., and W. H. Lipscomb, 2010: CICE: The Los Alamos Sea Ice Model documentation and software user's manual, version 4.1. Doc. LA-CC-06-012, 76 pp., http://csdms.colorado.edu/w/images/CICE_documentation_and_software_user's_manual.pdf.

Kim, H.-M., P. J. Webster, and J. A. Curry, 2012: Evaluation of short-term climate change prediction in multi-model CMIP5 decadal hindcasts. *Geophys. Res. Lett.*, **39**, L10701, https://doi.org/10.1029/2012GL051644.

Knudsen, M. F., B. H. Jacobsen, M.-S. Seidenkrantz, and J. Olsen, 2014: Evidence for external forcing of the Atlantic multidecadal oscillation since termination of the Little Ice Age. *Nat. Commun.*, **5**, 3323, https://doi.org/10.1038/ncomms4323.

Lee, J.-Y., and B. Wang, 2014: Future change of global monsoon in the CMIP5. *Climate Dyn.*, **42**, 101–119, https://doi.org/10.1007/s00382-012-1564-0.

Liu, F., J. Chai, B. Wang, J. Liu, X. Zhang, and Z. Wang, 2016: Global monsoon precipitation responses to large volcanic eruptions. *Sci. Rep.*, **6**, 24331, https://doi.org/10.1038/srep24331.

Liu, J., B. Wang, Q. Ding, X. Kuang, W. Soon, and E. Zorita, 2009: Centennial variations of the global monsoon precipitation in the last millennium: Results from ECHO-G model. *J. Climate*, **22**, 2356–2371, https://doi.org/10.1175/2008JCLI2353.1.

——, ——, S.-Y. Yim, J.-Y. Lee, J.-G. Jhun, and K.-J. Ha, 2012: What drives the global summer monsoon over the past millennium? *Climate Dyn.*, **39**, 1063–1072, https://doi.org/10.1007/s00382-012-1360-x.

Liu, Z., 2012: Dynamics of interdecadal climate variability: A historical perspective. *J. Climate*, **25**, 1963–1995, https://doi.org/10.1175/2011JCLI3980.1.

Livezey, R. E., and W. Y. Chen, 1983: Statistical field significance and its determination by Monte Carlo techniques. *Mon. Wea. Rev.*, **111**, 46–59, https://doi.org/10.1175/1520-0493(1983)111<0046:SFSAID>2.0.CO;2.

Lu, R., B. Dong, and H. Ding, 2006: Impact of the Atlantic multidecadal oscillation on the Asian summer monsoon. *Geophys. Res. Lett.*, **33**, L24701, https://doi.org/10.1029/2006GL027655.

Madec, G., 2008: NEMO ocean engine. Version 3.0, Note du Pôle de Modélisation 27, Institut Pierre-Simon Laplace, 209 pp.

Mantua, N. J., S. R. Hare, Y. Zhang, J. M. Wallace, and R. C. Francis, 1997: A Pacific interdecadal climate oscillation with impacts on salmon production. *Bull. Amer. Meteor. Soc.*, **78**, 1069–1079, https://doi.org/10.1175/1520-0477(1997)078<1069:APICOW>2.0.CO;2.

Martin, E. R., and C. Thorncroft, 2014: Sahel rainfall in multimodel CMIP5 decadal hindcasts. *Geophys. Res. Lett.*, **41**, 2169–2175, https://doi.org/10.1002/2014GL059338.

McCarthy, G. D., I. D. Haigh, J. J. M. Hirschi, J. P. Grist, and D. A. Smeed, 2015: Ocean impact on decadal Atlantic climate variability revealed by sea-level observations. *Nature*, **521**, 508–510, https://doi.org/10.1038/nature14491.

Meehl, G. A., 1987: The annual cycle and interannual variability in the tropical Pacific and Indian Ocean regions. *Mon. Wea. Rev.*, **115**, 27–50, https://doi.org/10.1175/1520-0493(1987)115<0027:TACAIV>2.0.CO;2.

——, and A. Hu, 2006: Megadroughts in the Indian monsoon region and southwest North America and a mechanism for associated multidecadal Pacific sea surface temperature anomalies. *J. Climate*, **19**, 1605–1623, https://doi.org/10.1175/JCLI3675.1.

——, and Coauthors, 2007: Global climate projection. *Climate Change 2007: The Physical Science Basis*, S. Solomon et al., Eds., Cambridge University Press, 747–846.

——, and Coauthors, 2014: Decadal climate prediction: An update from the trenches. *Bull. Amer. Meteor. Soc.*, **95**, 243–267, https://doi.org/10.1175/BAMS-D-12-00241.1.

Murphy, A. H., 1988: Skill scores based on the mean square error and their relationships to the correlation coefficient. *Mon. Wea. Rev.*, **116**, 2417–2424, https://doi.org/10.1175/1520-0493(1988)116<2417:SSBOTM>2.0.CO;2.

Murphy, L. N., K. Bellomo, M. Cane, and A. Clement, 2017: The role of historical forcings in simulating the observed Atlantic multidecadal oscillation. *Geophys. Res. Lett.*, **44**, 2472–2480, https://doi.org/10.1002/2016GL071337.

Otero, N., E. Mohino, and M. Gaetani, 2016: Decadal prediction of Sahel rainfall using dynamics-based indices. *Climate Dyn.*, **47**, 3415–3431, https://doi.org/10.1007/s00382-015-2738-3.

Polson, D., M. Bollasina, G. C. Hegerl, and L. J. Wilcox, 2014: Decreased monsoon precipitation in the Northern Hemisphere due to anthropogenic aerosols. *Geophys. Res. Lett.*, **41**, 6023–6029, https://doi.org/10.1002/2014GL060811.

Power, S., T. Casey, C. Folland, A. Colman, and V. Mehta, 1999: Inter-decadal modulation of the impact of ENSO on Australia. *Climate Dyn.*, **15**, 319–324, https://doi.org/10.1007/s003820050284.

Rayner, N. A., D. E. Parker, E. B. Horton, C. K. Folland, L. V. Alexander, D. P. Rowell, E. C. Kent, and A. Kaplan, 2003: Global analyses of sea surface temperature, sea ice, and night marine air temperature since the late nineteenth century. *J. Geophys. Res.*, **108**, 4407, https://doi.org/10.1029/2002JD002670.

Roeckner, E., and Coauthors, 1996: The atmospheric general circulation model ECHAM4: Model description and simulation of the present-day climate. MPI für Meteorologie Tech. Rep. 31813, 90 pp.

Schneider, T., T. Bischoff, and G. H. Haug, 2014: Migrations and dynamics of the intertropical convergence zone. *Nature*, **513**, 45–53, https://doi.org/10.1038/nature13636.

Smith, T. M., P. A. Arkin, M. R. P. Sapiano, and C.-Y. Chang, 2010: Merged statistical analyses of historical monthly precipitation anomalies beginning 1900. *J. Climate*, **23**, 5755–5770, https://doi.org/10.1175/2010JCLI3530.1.

Sutton, R. T., and D. L. R. Hodson, 2005: Atlantic Ocean forcing of North American and European summer climate. *Science*, **309**, 115–118, https://doi.org/10.1126/science.1109496.

Taylor, K. E., R. J. Stouffer, and G. A. Meehl, 2012: An overview of CMIP5 and the experiment design. *Bull. Amer. Meteor. Soc.*, **93**, 485–498, https://doi.org/10.1175/BAMS-D-11-00094.1.

Uppala, S. M., and Coauthors, 2005: The ERA-40 re-analysis. *Quart. J. Roy. Meteor. Soc.*, **131**, 2961–3012, https://doi.org/10.1256/qj.04.176.

van Oldenborgh, G. J., F. J. Doblas-Reyes, B. Wouters, and W. Hazeleger, 2012: Decadal prediction skill in a multi-model ensemble. *Climate Dyn.*, **38**, 1263–1280, https://doi.org/10.1007/s00382-012-1313-4.

Wang, B., and Q. Ding, 2006: Changes in global monsoon precipitation over the past 56 years. *Geophys. Res. Lett.*, **33**, L06711, https://doi.org/10.1029/2005GL025347.

——, and ——, 2008: Global monsoon: Dominant mode of annual variation in the tropics. *Dyn. Atmos. Oceans*, **44**, 165–183, https://doi.org/10.1016/j.dynatmoce.2007.05.002.

——, I. S. Kang, and J. Y. Lee, 2004: Ensemble simulations of Asian–Australian monsoon variability by 11 AGCMs. *J. Climate*, **17**, 803–818, https://doi.org/10.1175/1520-0442(2004)017<0803:ESOAMV>2.0.CO;2.

——, Q. Ding, X. Fu, I. S. Kang, K. Jin, J. Shukla, and F. Doblas-Reyes, 2005: Fundamental challenge in simulation and prediction of summer monsoon rainfall. *Geophys. Res. Lett.*, **32**, L15711, https://doi.org/10.1029/2005GL022734.

——, J. Liu, H.-J. Kim, P. Webster, and S.-Y. Yim, 2012: Recent change of the global monsoon precipitation (1979–2008). *Climate Dyn.*, **39**, 1123–1135, https://doi.org/10.1007/s00382-011-1266-z.

——, ——, ——, P. J. Webster, S.-Y. Yim, and B. Xiang, 2013: Northern Hemisphere summer monsoon intensified by mega-El Niño/Southern Oscillation and Atlantic multidecadal oscillation. *Proc. Natl. Acad. Sci. USA*, **110**, 5347–5352, https://doi.org/10.1073/pnas.1219405110.

——, B. Xiang, J. Li, P. J. Webster, M. N. Rajeevan, J. Liu, and K.- J. Ha, 2015: Rethinking Indian monsoon rainfall prediction in the context of recent global warming. *Nat. Commun.*, **6**, 7154, https://doi.org/10.1038/ncomms8154.

Webster, P. J., and J. Jian, 2011: Environmental prediction, risk assessment and extreme events: Adaptation strategies for the developing world. *Philos. Trans. Roy. Soc. London*, **369A**, 4768–4797, https://doi.org/10.1098%2Frsta.2011.0160.

——, V. O. Magaña, T. N. Palmer, J. Shukla, R. A. Tomas, M. Yanai, and T. Yasunari, 1998: Monsoons: Processes, predictability, and the prospects for prediction. *J. Geophys. Res.*, **103**, 14451–14510, https://doi.org/10.1029/97JC02719.

Yasunari, T., 1991: The monsoon year—A new concept of the climatic year in the tropics. *Bull. Amer. Meteor. Soc.*, **72**, 1331–1338, https://doi.org/10.1175/1520-0477(1991)072<1331:TMYNCO>2.0.CO;2.

Yim, S.-Y., B. Wang, J. Liu, and Z. Wu, 2014: A comparison of regional monsoon variability using monsoon indices. *Climate Dyn.*, **43**, 1423–1437, https://doi.org/10.1007/s00382-013-1956-9.

Zhang, R., and T. L. Delworth, 2006: Impact of Atlantic multidecadal oscillations on India/Sahel rainfall and Atlantic hurricanes. *Geophys. Res. Lett.*, **33**, L17712, https://doi.org/10.1029/2006GL026267.

Zhou, T., R. Yu, H. Li, and B. Wang, 2008: Ocean forcing to changes in global monsoon precipitation over the recent half-century. *J. Climate*, **21**, 3833–3852, https://doi.org/10.1175/2008JCLI2067.1.